J Supercond Nov Magn (2015) 28:3163–3172
DOI 10.1007/s10948-015-3148-9

ORIGINAL PAPER

Half-Metallic Ferromagnetic Property Related to Spintronic Applications in 3*d* (V, Cr, and Mn)-Doped GaP DMSs

B. Doumi[1,2] · A. Mokaddem[3] · A. Sayede[4] · M. Boutaleb[1] · A. Tadjer[1] · F. Dahmane[5]

Received: 26 March 2015 / Accepted: 16 June 2015 / Published online: 30 June 2015

Abstract Using the full-potential linearized augmented plane-wave method of first-principles calculations of density functional theory, we have performed a systematic investigations on the structural, electronic, and magnetic properties related to the spintronic applications for gallium phosphide GaP doped with 3*d* transition metal (TM) atoms such as vanadium (V), chromium (Cr), and manganese (Mn) as ternary $Ga_{1-x}TM_xP$ diluted magnetic semiconductors (DMSs) in zinc-blende phase at concentrations $x = 0.0625$, 0.125, and 0.25. The analysis of electronic and magnetic properties with various concentrations (x) of TM revealed that $Ga_{1-x}V_xP$ at ($x = 0.0625$, 0.125, and 0.25) and $Ga_{1-x}TM_xP$ (TM = Cr and Mn) at ($x = 0.0625$ and 0.125) are half-metallic ferromagnets (HMF) with spin polarization of 100 %. The HMF character destroyed for $Ga_{1-x}Cr_xP$ and $Ga_{1-x}Mn_xP$ at higher concentration $x = 0.25$ of Cr and Mn. The half-metallic gap increases with decreasing in concentration of impurity, and therefore, the $Ga_{1-x}TM_xP$, $Ga_{1-x}Cr_xP$, and $Ga_{1-x}Mn_xP$ DMSs at low concentrations appear to be better candidates for spintronic applications.

Keywords Spintronics · Electronic structure · Half-metallic ferromagnetism · Half-metallic gap · (V, Cr, and Mn)-doped GaP

✉ B. Doumi
bdoummi@yahoo.fr

1 Modelling and Simulation in Materials Science Laboratory, Physics Department, Djillali Liabes University of Sidi Bel-Abbes, 22000 Sidi Bel-Abbes, Algeria

2 Faculty of Sciences, Department of Physics, Dr. Tahar Moulay University of Saïda, 20000 Saïda, Algeria

3 Faculty of Physics, Department of Materials and Components, U.S.T.H.B., Algiers, Algeria

4 Unité de Catalyse et Chimie du Solide (UCCS), UMR CNRS 8181, Faculté des Sciences, Université d'Artois, Rue Jean Souvraz, SP 18, 62307 Lens, France

5 Institut des Sciences et Technologies, Département sciences de la matière, Centre, Universitaire Tissemsilt, Tissemsilt 38000, Algérie

1 Introduction

Spintronics, also known as magnetoelectronics, is a new generation of microelectronics and involves utilizing both charge and spin degrees of freedom of electrons [1]. During the past decade, the development of diluted magnetic semiconductors (DMSs) for spintronics made revolution in the processing and storage information technologies. The half-metallic ferromagnets DMSs based on III–V doped with transition metals are the main ingredients of high-performance spintronic devices in the future [2, 3], because they are characterized with Curie temperature higher than room temperature and half-metallic ferromagnetic (HMF) behavior [4]. They have a band gap at the Fermi level for only one spin direction and conductor only from the charge carriers of the other spin channel [5]. Thus, the HMF character takes a significant role in the progress of new materials for the spintronic devices, especially as a source of spin-polarized injected carriers in the DMSs [6]. Recently, several theoretical works [7–24] focused on the investigation of HMF DMSs-based on II–VI and III–V semiconductors doped with transition metal elements in the intention to predict their use in the spintronic applications; further, new experimental studies were carried out in this area [25–30].

Table 1 Calculated of lattice constant (a), bulk modulus (B), and its pressure derivative (B') for GaP, and $Ga_{1-x}TM_xP$ (TM = V, Cr, and Mn) at concentrations ($x = 0.0625$, 0.125, and 0.25)

Compound	Concentration (x)	a (Å)	B(GPa)	B'	Method
This work					GGA-WC
GaP	0.00	5.446	85.96	4.55	
$Ga_{1-x}V_xP$	0.0625	5.436	86.31	4.89	
	0.125	5.434	87.80	4.09	
	0.25	5.429	88.04	4.22	
$Ga_{1-x}Cr_xP$	0.0625	5.423	87.306	4.83	
	0.125	5.413	88.36	4.29	
	0.25	5.382	91.78	4.28	
$Ga_{1-x}Mn_xP$	0.0625	5.416	87.20	4.55	
	0.125	5.397	89.40	4.47	
	0.25	5.351	93.55	4.68	
Other calculations					
GaP	0.00	5.448 [44]	85.50 [44]		GGA-WC
		5.451 [45]	88.00 [46]		Experimental
$Ga_{1-x}Cr_xP$	0.0625	5.517 [9]			GGA-PBE
	0.125	5.439 [8], 5.512 [9]			GGA-PBE
	0.25	5.435 [8], 5.501 [9]			GGA-PBE
$Ga_{1-x}Mn_xP$	0.125	5.470 [10]			GGA-WC

The GaP is an important semiconductor that belongs to III–V group, which crystallizes in the zinc-blende phase with a wide indirect band gap [31]. It has received significant attention as a material for exploitation in a wide range of important modern optoelectronic devices including photodetectors, light emitters, electroluminescent displays, and power diodes as well as being a model material with which to investigate the fundamental properties of semiconductors

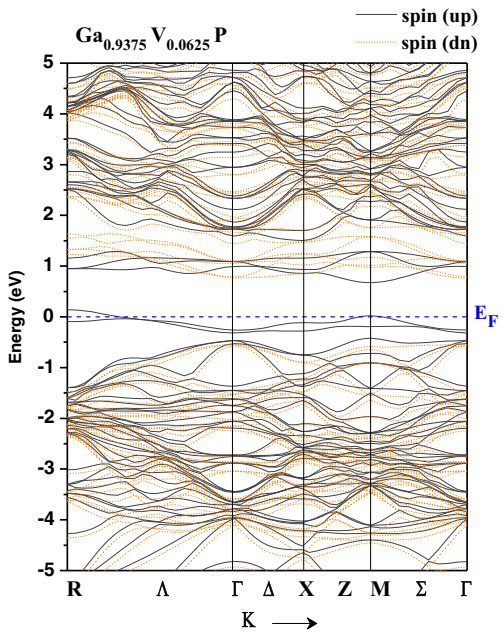

Fig. 1 Spin-polarized band structures for majority spin (*up*) and minority spin (*dn*) for $Ga_{0.9375}V_{0.0625}P$. The Fermi level is set to zero (*dotted line*) (color figure online)

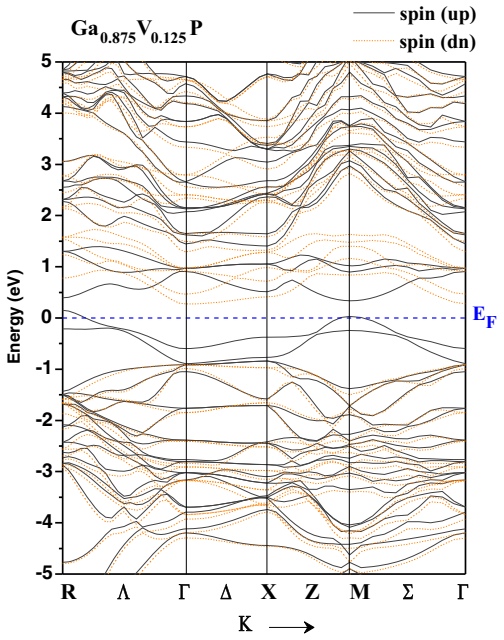

Fig. 2 Spin-polarized band structures for majority spin (*up*) and minority spin (*dn*) for $Ga_{0.875}V_{0.125}P$. The Fermi level is set to zero (*dotted line*) (color figure online)

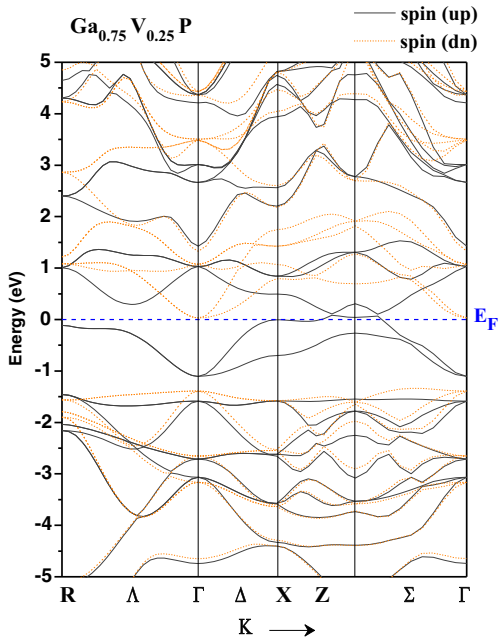

Fig. 3 Spin-polarized band structures for majority spin (*up*) and minority spin (*dn*) for $Ga_{0.75}$ $V_{0.25}P$. The Fermi level is set to zero (*dotted line*) (color figure online)

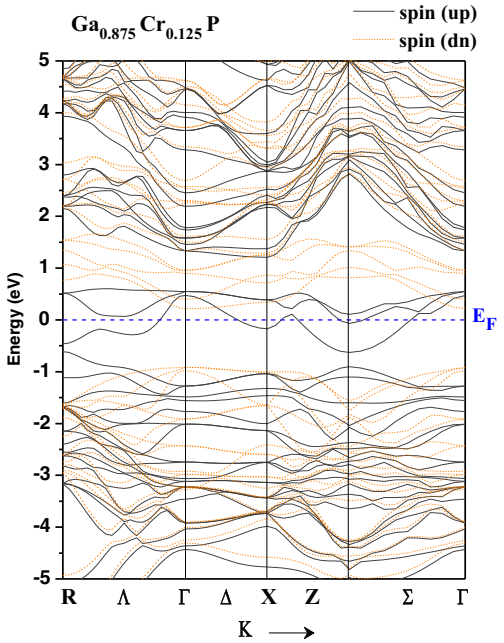

Fig. 5 Spin-polarized band structures for majority spin (*up*) and minority spin (*dn*) for $Ga_{0.875}Cr_{0.125}P$. The Fermi level is set to zero (*dotted line*) (color figure online)

[32]. However, T. Dietl et al. [33] predicted that the *p*-type GaMnP DMS has a Curie temperature (T_C) of roughly 100 K, and the manganese (Mn) plays a special role in the III-Mn–V compounds, as it is a relatively deep acceptor, whose level is 0.39 eV above the valence band maximum in GaP [34]. Although, several experimental studies considered gallium phosphide doped with manganese a best candidate as a DMS, M. A. Scarpulla et al. [35] reported that

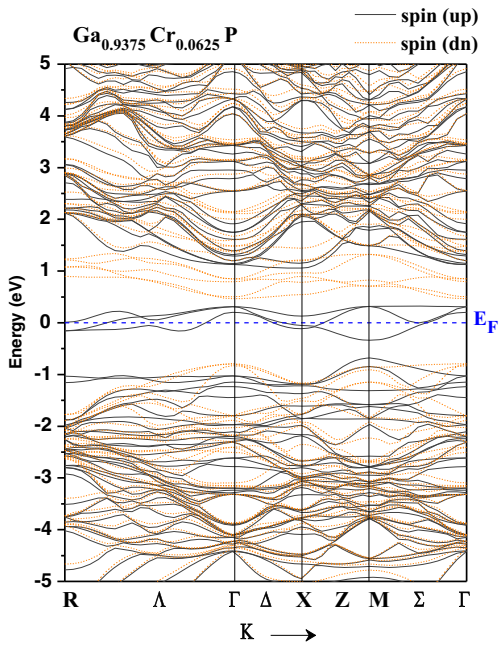

Fig. 4 Spin-polarized band structures for majority spin (*up*) and minority spin (*dn*) for $Ga_{0.9375}Cr_{0.0625}P$. The Fermi level is set to zero (*dotted line*) (color figure online)

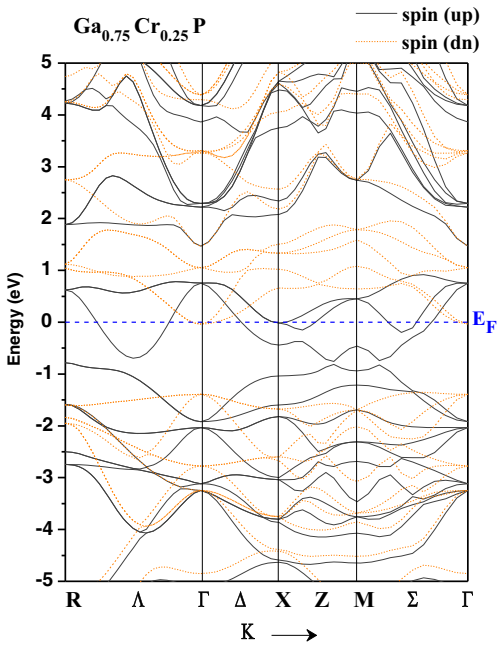

Fig. 6 Spin-polarized band structures for majority spin (*up*) and minority spin (*dn*) for $Ga_{0.75}Cr_{0.25}P$. The Fermi level is set to zero (*dotted line*) (color figure online)

$Ga_{1-x}Mn_xP$ represents a novel DMS alloy system where strongly localized carriers in a detached impurity band stabilize ferromagnetism, and F.J. Owens [36] found by both ferromagnetic resonance and AC magnetization measurements the existence of ferromagnetism in GaP hole doped with 3 % Mn and having a Curie temperature of 600 K. In addition, the half-metallic ferromagnetism has been theoretically predicted in $Ga_{1-x}Cr_xP$ ($x = 0.125$, 0.25, and 0.5) [8], $Ga_{1-x}Cr_xP$ ($x = 0.03$, 0.06, 0.125, and 0.25) [9], $Ga_{0.875}Mn_{0.125}P$ [10], and $Ga_{0.875}Cr_{0.125}P$ [11].

The aim of the present work is to study the ternary $Ga_{1-x}TM_xP$ (TM = V, Cr, and Mn) DMSs, which the transition metal impurities (TM = V, Cr, and Mn)-doped GaP semiconductor give a particular half-metallic ferromagnetic property with 100 % spin polarization. We have explored the structural, electronic, and magnetic properties of $Ga_{1-x}TM_xP$ (TM = V, Cr, and Mn) at concentrations $x = 0.0625$, 0.125, and 0.25, using first-principles calculations of density functional theory [37, 38] within the framework of full-potential linearized augmented plane-wave (FP-LAPW) method with generalized gradient approximation functional proposed by Wu and Cohen (GGA-WC) [39].

2 Method and Details of Calculations

The calculations are performed in the framework of the density functional theory (DFT) [37, 38] within the full-potential linearized augmented plane wave (FP-LAPW) method as implemented in the WIEN2k code [40]. The generalized gradient approximation functional proposed by Wu and Cohen (GGA-WC) was used for the exchange correlation potential [39] to investigate the electronic and half-metallic ferromagnetic properties of (TM = V, Cr, and Mn)-doped GaP in zinc-blende (B3) structure, based on $Ga_{15}TMP_{16}$, Ga_7TMP_8, and Ga_3TMP_4 supercells of 32, 16, and 8 atoms, respectively. The GaP has a zinc-blende structure with space group $F\bar{4}3m$, where the Ga atom is located at position (0, 0, 0) and P atom at (0.25, 0.25, 0.25). The $Ga_{1-x}TM_xP$ (TM = V, Cr, and Mn) compounds with concentrations $x = 0.0625$, 0.125, and 0.25 are obtained by substituted one Ga atom with one (TM) atom in supercells of 32, 16, and 8 atoms, respectively. We get the $Ga_{0.9375}TM_{0.0625}P$ ($1 \times 2 \times 2$) supercell of 32 atoms with $x = 0.0625$ of tetragonal structure with space group $P\bar{4}2m$, $Ga_{0.875}TM_{0.125}P$ ($1 \times 1 \times 2$) supercell of 16 atoms with $x = 0.125$ of tetragonal structure with space group $P\bar{4}2m$, and $Ga_{0.75}TM_{0.25}P$ ($1 \times 1 \times 1$) supercell of 8 atoms with $x = 0.25$ of cubic structure with space group $P\bar{4}3m$.

We have taken the averages of non-overlapping muffin–tin radii (R_{MT}) of Ga, P, V, Cr, and Mn in such a way that the muffin-tin spheres do not overlap. We have expanded

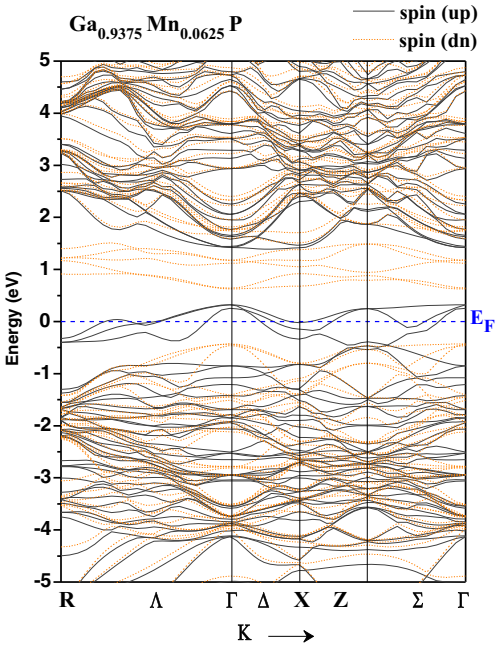

Fig. 7 Spin-polarized band structures for majority spin (*up*) and minority spin (*dn*) for $Ga_{0.9375}Mn_{0.0625}P$. The Fermi level is set to zero (*dotted line*) (color figure online)

the wave functions in the interstitial region to plane waves with a cutoff of $K_{max} = 8.0/R_{MT}$ (where K_{max} is the magnitude of the largest K vector in the plane wave and R_{MT} is the average radius of the muffin–tin spheres), and the maximum value for partial waves inside the atomic sphere was

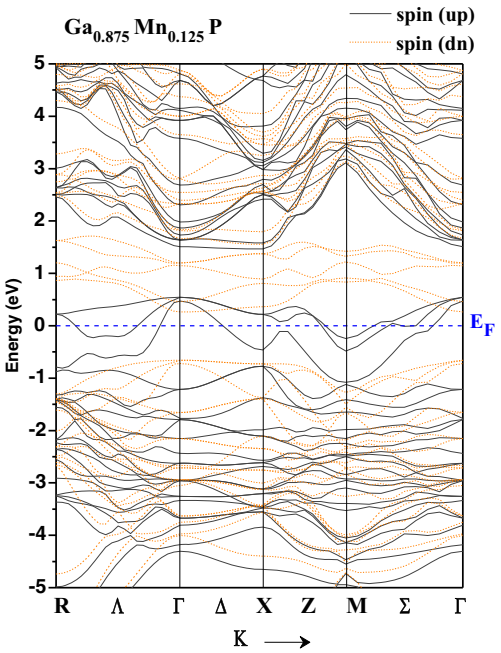

Fig. 8 Spin-polarized band structures for majority spin (*up*) and minority spin (*dn*) for $Ga_{0.875}Mn_{0.125}P$. The Fermi level is set to zero (*dotted line*) (color figure online)

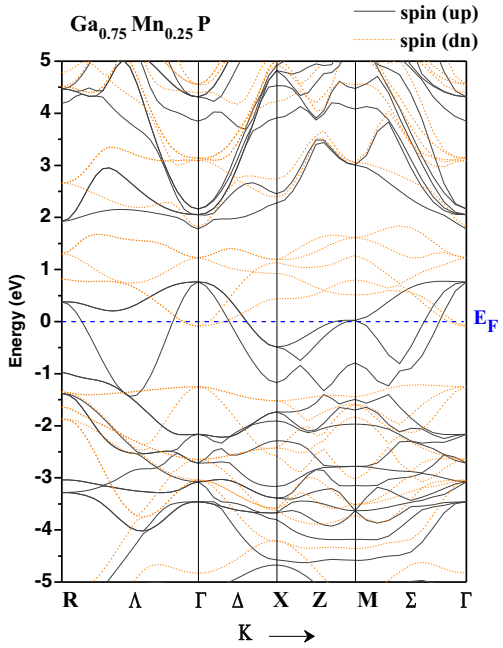

Fig. 9 Spin-polarized band structures for majority spin (*up*) and minority spin (*dn*) for $Ga_{0.75}Mn_{0.25}P$. The Fermi level is set to zero (*dotted line*) (color figure online)

$l_{max} = 10$, while the charge density was Fourier expanded up to $G_{max} = 12$ a.u.$^{-1}$, where G_{max} is the largest vector in the Fourier expansion. The energy cutoff was chosen as - 6 Ry, which defines the separation of valence and core states. For the sampling of the Brillouin zone, (4 × 4 × 4), (4×4×2), and (2×2×5) Monkhorst–Pack mesh [41, 42] are utilized for supercells of 32, 16, and 8 atoms, respectively, where the self-consistent convergence of the total energy was at 0.1 mRy.

3 Results and Discussions

3.1 Optimization of Structures

To determine the analysis of the electronic and magnetic properties of $Ga_{1-x}TM_xP$ (TM = V, Cr, and Mn) compounds, we calculated firstly the structural properties of compounds. The $Ga_{1-x}V_xP$, $Ga_{1-x}Cr_xP$, and $Ga_{1-x}Mn_xP$ supercells are optimized by fitting empirical Murnaghan's equation of state [43] of the variations of total energies as a function of equilibrium volumes. Our results of the equilibrium lattice constants (a), bulk modules (B) and its pressure derivatives (B') of $Ga_{1-x}TM_xP$ (TM = V, Cr, and Mn) compounds, various theoretical [8–10, 44], and experimental [45, 46] data are given in Table 1.

The computed lattice constant (a = 5.446 Å) of GaP is very close to the theoretical value (5.448 Å) [44] by the same GGA-WC method [39] and stays in good agreement with experimental ones [45]. For the $Ga_{1-x}TM_xP$ (TM = V, Cr, and Mn), we observed that the lattice constants decrease as the concentration of TM increases due to the smaller atomic radii of V, Cr, and Mn compared to the Ga atom, which signify that the local structure around the (V, Cr, and Mn) doping is slightly suppressed with the P atoms drawn closer to the (V, Cr, and Mn) atoms. We noticed that our computed lattice parameters of $Ga_{1-x}Cr_xP$ and $Ga_{1-x}Mn_xP$ with GGA-WC [39] are better than the theoretical calculations [8–10] with generalized

Table 2 Calculated half-metallic ferromagnetic band gapE_g, half-metallic gap G_{hm} of minority spin, and half-metallic ferromagnetic (HMF) or metallic ferromagnetic (MF) behavior for $Ga_{1-x}TM_xP$ (TM = V, Cr, and Mn) at concentrations (x = 0.0625, 0.125, and 0.25)

Compound	Concentration (x)	E_g (eV)	G_{hm} (eV)	Behavior
This work				
$Ga_{1-x}V_xP$	0.0625	1.309	0.546	HMF
	0.125	1.192	0.273	HMF
	0.25	1.417	0.027	HMF
$Ga_{1-x}Cr_xP$	0.0625	1.261	0.464	HMF
	0.125	1.133	0.216	HMF
	0.25	–	–	MF
$Ga_{1-x}Mn_xP$	0.0625	1.049	0.430	HMF
	0.125	0.921	0.262	HMF
	0.25	–	–	MF
Other theoretical calculations				
$Ga_{1-x}Cr_xP$	0.0625	–	0.712 [9]	HMF
	0.125	1.350 [8]	0.470 [8], 0.451 [9]	HMF
	0.25	1.460 [8]	0.280 [8], 0.301 [9]	HMF
$Ga_{1-x}Mn_xP$	0.125	1.200 [11]	0.150 [11]	HMF

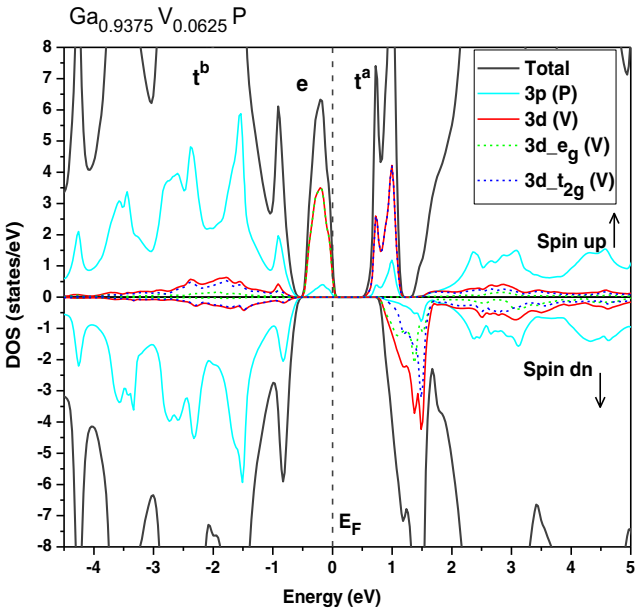

Fig. 10 Spin-polarized total and partial DOS of ($3p$) of P and ($3d$, $3d$–e_g, $3d$–$_g$) of V in supercell for $Ga_{0.9375}V_{0.0625}P$. The Fermi level is set to zero (*dotted line*) (color figure online)

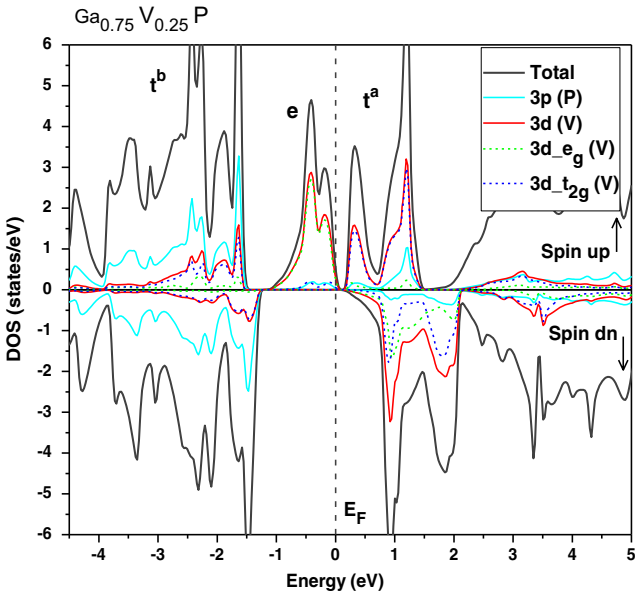

Fig. 12 Spin-polarized total and partial DOS of ($3p$) of P and ($3d$, $3d$–e_g, $3d$–t_{2g}) of V in supercell for $Ga_{0.75}V_{0.25}P$. The Fermi level is set to zero (*dotted line*) (color figure online)

gradient approximation of Perdew, Burke, and Ernzerhof (GGA-PBE) [47] due to better performance of GGA-WC approximation for structural optimization [22, 24, 48]. The calculated bulk modules of $Ga_{1-x}V_xP$, $Ga_{1-x}Cr_xP$ and $Ga_{1-x}Mn_xP$ increase with increasing of concentrations (x) of V, Cr, and Mn atoms, and this suggests that the compressibilityof each compound increases with the increases in the concentration (x) of TM, and therefore the $Ga_{1-x}TM_xP$ compounds become harder as the concentrations of vanadium, chromium, and manganese increase.

3.2 Electronic Properties with Half-Metallic Behavior

The plots of the spin-polarized band structures of $Ga_{1-x}V_xP$, $Ga_{1-x}Cr_xP$, and $Ga_{1-x}Mn_xP$ with different concentrations ($x = 0.0625$, 0.125, and 0.25) are presented

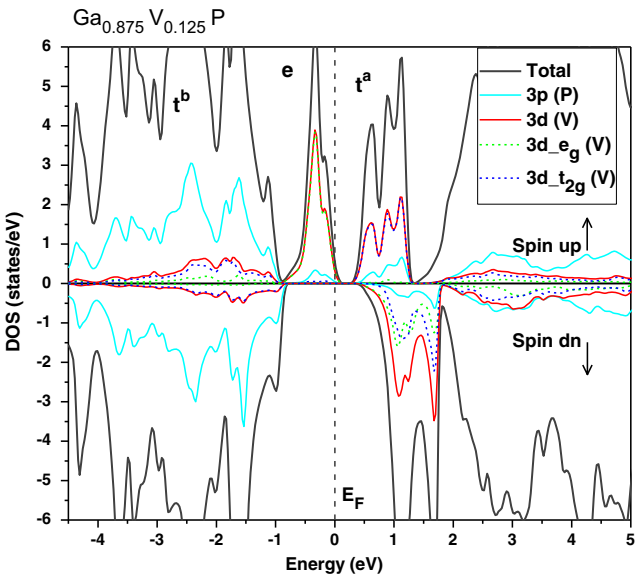

Fig. 11 Spin-polarized total and partial DOS of ($3p$) of P and ($3d$, $3d$–e_g, $3d$–t_{2g}) of V in supercell for $Ga_{0.875}V_{0.125}P$. The Fermi level is set to zero (*dotted line*) (color figure online)

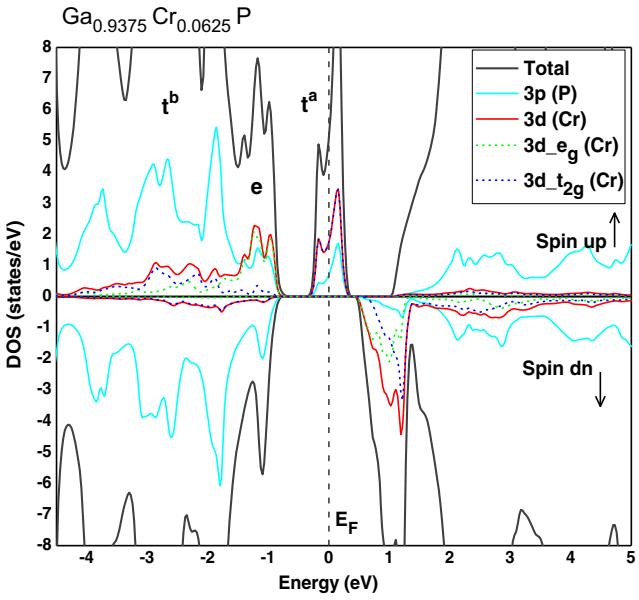

Fig. 13 Spin-polarized total and partial DOS of ($3p$) of P and ($3d$, $3d$–e_g, $3d$–t_{2g}) of Cr in supercell for $Ga_{0.9375}Cr_{0.0625}P$. The Fermi level is set to zero (*dotted line*) (color figure online)

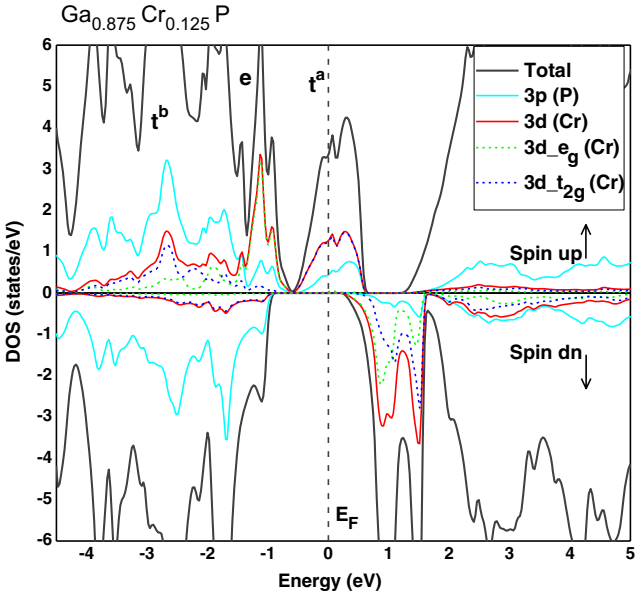

Fig. 14 Spin-polarized total and partial DOS of (3*p*) of P and (3*d*, 3*d*–e_g, 3*d*–t_{2g}) of Cr in supercell for $Ga_{0.875}Cr_{0.125}P$. The Fermi level is set to zero (*dotted line*) (color figure online)

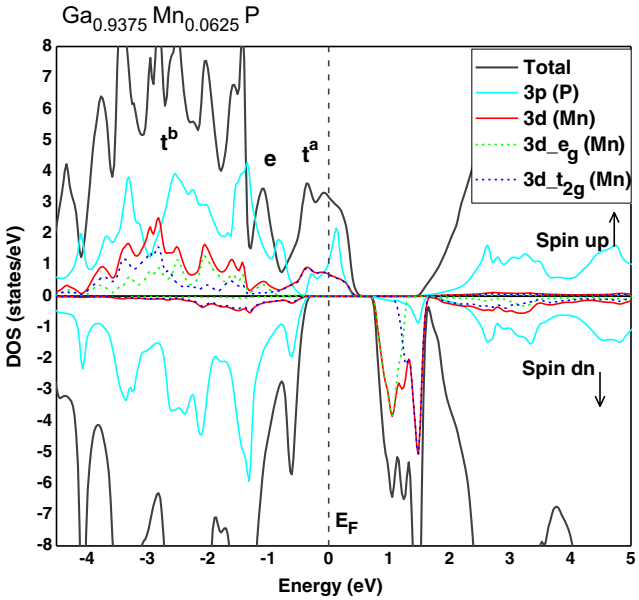

Fig. 16 Spin-polarized total and partial DOS of (3*p*) of P and (3*d*, 3*d*–e_g, 3*d*–t_{2g}) of Mn in supercell for $Ga_{0.9375}Mn_{0.0625}P$. The Fermi level is set to zero (*dotted line*) (color figure online)

by Figs. 1, 2, 3, 4, 5, 6, 7, 8, and 9. They depicted that the top of valance band of the majority-spin crosses the Fermi level, while the minority-spin bands show a band gap around the Fermi level for $Ga_{1-x}V_xP$ at concentrations ($x = 0.0625$, 0.125, and 0.25) and $Ga_{1-x}TM_xP$ (TM = Cr and Mn) at ($x = 0.0625$ and 0.125). Consequently, these compounds show a half-metallic ferromagnetic (HMF) behavior. In contrast, the half-metallicity destroyed for $Ga_{1-x}Cr_xP$ and $Ga_{1-x}Mn_xP$ at higher concentration $x = 0.25$ because the majority-spin bands are metallic whereas for the minority spin bands the minimum of the conduction band broad strongly in the gap, resulting in metallic character, and thus the $Ga_{1-x}TM_xP$ (TM = Cr and Mn) at $x = 0.25$ are metallic in nature.

Furthermore, for the HMF compounds the minority-spin bands exhibit two gaps; a half-metallic ferromagnetic

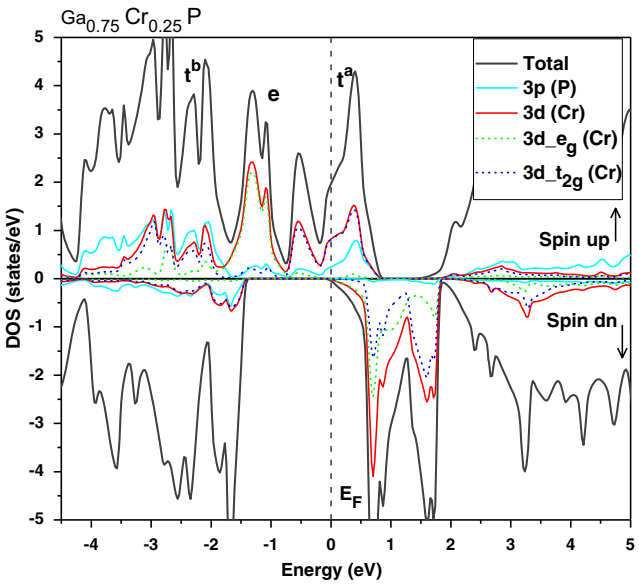

Fig. 15 Spin-polarized total and partial DOS of (3*p*) of P and (3*d*, 3*d*–e_g, 3*d*–t_{2g}) of Cr in supercell for $Ga_{0.75}Cr_{0.25}P$. The Fermi level is set to zero (*dotted line*) (color figure online)

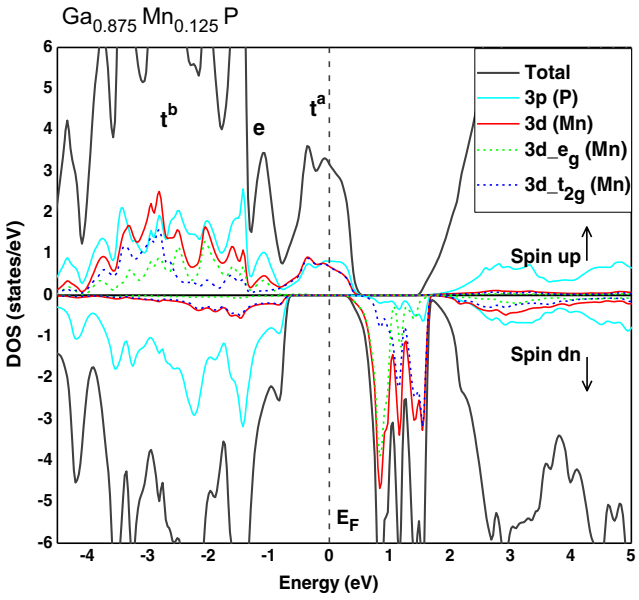

Fig. 17 Spin-polarized total and partial DOS of (3*p*) of P and (3*d*, 3*d*–e_g, 3*d*–t_{2g}) of Mn in supercell for $Ga_{0.875}Mn_{0.125}P$. The Fermi level is set to zero (*dotted line*) (color figure online)

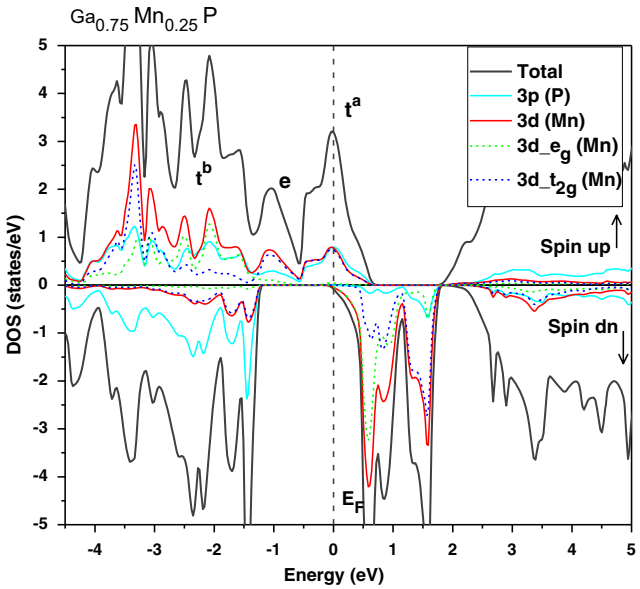

Fig. 18 Spin-polarized total and partial DOS of ($3p$) of P and ($3d$, $3d$–e_g, $3d$–t_{2g}) of Mn in supercell for $Ga_{0.75}Mn_{0.25}P$. The Fermi level is set to zero (*dotted line*) (color figure online)

(HMF) gap (E_g) and a half-metallic (HM) gap (G_{hm}). The HM gap is considered an important parameter to determine the application in spintronics [4], which is defined as the minimum between the lowest energy of majority (minority)-spin conduction bands with respect to the Fermi level, and the absolute values of the highest energy of majority (minority)-spin valence bands [49, 50]. The calculated HMF gap E_g and the HM gap G_{hm} of minority-spin channels with different concentrations are shown in Table 2. Our results show that the both HMF gap and HM gap decrease due to the broadening of the $3d$ (V, Cr, and Mn) bands in the gap as the concentrations of (V, Cr, and Mn) impurities increase. For $Ga_{1-x}Cr_xP$ at concentrations $x = 0.0625$ and 0.125 and $Ga_{1-x}Mn_xP$ at $x = 125$, the HMF gaps and HM gaps are lower than the other theoretical calculations [8, 9] due to the difference between our computed equilibrium lattice constants by the GGA-WC exchange correlation potential [39] and those found by GGA-PBE method [47]. Moreover, the minimal energy gap for a spin excitation is described by the HM gap [51], which has high values of 0.546, 4.64, and 0.43 eV at the lower concentration $x = 0.0625$ respectively for $Ga_{1-x}V_xP$, $Ga_{1-x}Cr_xP$, and $Ga_{1-x}Mn_xP$. The wide HM gap suggests a true half metallic ferromagnet and makes the $Ga_{1-x}TM_xP$ (TM = V, Cr, and Mn) at low concentration potential candidates for spintronic applications.

The total (T) and partial (P) density of states (DOS) p of (Ga and P) and $3d$ (t_{2g}, e_g) of (TM = V, Cr, and Mn) for $Ga_{1-x}TM_xP$ with different concentrations (x) are display by Figs. 10, 11, 12, 13, 14, 15, 16, 17, and 18. The $3d$(V, Cr, and Mn) minority-spin states are located above Fermi level, indicating that these states are empty, whereas the majority-spin states show strong hybridization between $3d$ (V, Cr, and Mn) and $3p$ (P) states that make the upper part of valence band. In this case, the t_{2g} states are situated above Fermi level for V atom, while they dominated the Fermi level for (Cr and Mn), and thus the $3d - t_{2g}$

Table 3 Calculated total and local magnetic moment (in Bohr magneton μ_B) within the muffin–tin spheres and in the interstitial sites for $Ga_{1-x}TM_xP$ (TM = V, Cr, and Mn) at concentrations ($x = 0.0625$, 0.125, and 0.25)

Compound	Concentration (x)	Total (μ_B)	V/Cr/Mn (μ_B)	Ga (μ_B)	P (μ_B)	Interstitial (μ_B)
This work						
$Ga_{1-x}V_xP$	0.0625	2	1.581	0.081	−0.109	0.487
	0.125	2	1.628	0.046	−0.096	0.372
	0.25	2	1.639	0.078	−0.094	0.390
$Ga_{1-x}Cr_xP$	0.0625	3	2.598	0.104	−0.220	0.602
	0.125	3	2.662	0.053	−0.189	0.470
	0.25	3	2.643	0.092	−0.184	0.480
$Ga_{1-x}Mn_xP$	0.0625	4	3.395	0.085	−0.095	0.646
	0.125	4	3.441	0.063	−0.118	0.580
	0.25	4	3.382	0.099	−0.519	0.574
Other theoretical calculations						
$Ga_{1-x}Cr_xP$	0.0625	3.003 [9]	2.851 [9]	0.005 [9]	−0.022 [9]	0.343 [9]
	0.125	3.000 [8]	2.735 [8]	0.018 [8]	−0.049 [8]	
		3.012 [9]	2.856 [9]	0.012 [9]	−0.034 [9]	0.341 [9]
	0.25	3.000 [8]	2.761 [8]	0.031 [8]	−0.054 [8]	
		3.002 [9]	2.847 [9]	0.028 [9]	−0.065 [9]	0.329 [9]
$Ga_{1-x}Mn_xP$	0.125	4.000 [10]	3.594 [10]	–	−0.0245 [10]	0.438 [10]

(TM) states are unoccupied and partially filled states respectively for $Ga_{1-x}V_xP$ and $Ga_{1-x}TM_xP$ (TM = Cr and Mn). However, in the DMS materials, the stabilization of ferromagnetic state is explained by the double-exchange mechanism when the delocalized anti-bonding states are partially occupied [52–54], and in the case of $Ga_{1-x}TM_xP$ (TM = V, Cr, and Mn) doping systems, the partially filled $3d$–t_{2g} (V, Cr, and Mn) majority-spin states suggest a ferromagnetic ground state associated with the double-exchange mechanism [55]. From the curves of the densities of states, we noted that $Ga_{1-x}V_xP$ at concentrations ($x = 0.0625$, 0.125, and 0.25) and $Ga_{1-x}TM_xP$ (TM = Cr and Mn) at ($x = 0.0625$ and 0.125) exhibit a half-metallic ferromagnetic character, this amounts to the presence of band gap in the minority spin and metallic nature of the majority spin that is a consequence of the strong p-d hybridization between two states as $3p$ (P) anions and $3d$ (V, Cr, and Mn) impurities. In contrast, for $Ga_{1-x}Cr_xP$ and $Ga_{1-x}Mn_xP$ at higher concentration $x = 0.25$, the $3d$ (Cr, and Mn) minority-spin states broaden strongly in the gap and cross the Fermi level, and hence these compounds are metallic ferromagnets.

3.3 Magnetic Properties

The computed total and local magnetic moments in the muffin–tin spheres and in the interstitial sites of the relevant (Ga, P) and transition metal (TM = V, Cr, Mn) atoms for all compounds are given in Table 3. In the $Ga_{1-x}TM_xP$ DMSs, the each TM atom contributes three electrons to bonding states, and therefore the electronic configuration of tetrahedrally bonded (TM = V, Cr, and Mn) in $Ga_{1-x}TM_xP$ systems are V^{+3} ($d^2 - e_g^2 t_{2g}^0$), Cr^{+3} ($d^3 - e_g^2 t_{2g}^1$), and Mn^{+3} ($d^4 - e_g^2\ t_{2g}^2$). Based to Hund's rule, the $3d$ (TM) majority-spin states are partially filled with two, three, and four electrons, respectively for V, Cr and Mn. This creates total magnetic moments of 2, 3, and 4 μ_B (μ_B is the Bohr magneton) respectively for $Ga_{1-x}V_xP$ at concentrations ($x = 0.0625$, 0.125, and 0.25), $Ga_{1-x}Cr_xP$ at ($x = 0.0625$ and 0.125), and $Ga_{1-x}Mn_xP$ at ($x = 0.0625$ and 0.125), and hence these DMSs are true half-metallic ferromagnets.

Table 3 depicts that the magnetic moments of transition metal (V, Cr, and Mn) impurities are inferior to those predicted by Hund's rule due to the p-d hybridization [18, 22, 23]. However, the major contributions of total magnetic moments are localized around the (V, Cr, and Mn) atoms and smaller local magnetic moments are induced in (Ga, P) and interstitial sites. The negative signs of the magnetic moments of (P) atoms revealed the anti-ferromagnetic interaction between valence band and $3d$ (V, Cr, and Mn) spins, while the ferromagnetic interaction is shown between Ga and $3d$ (V, Cr, and Mn) magnetic spins.

4 Conclusion

In this study, we have investigated the structural, electronic, and half-metallic ferromagnetic properties of $Ga_{1-x}TM_xP$ (TM = V, Cr, and Mn) DMSs in zinc-blende phase at various concentrations $x = 0.0625$, 0.125, and 0.25 by using the FP-LAPW method within first-principles calculations of density functional theory with GGA-WC approximation. We found that $Ga_{1-x}V_xP$ at concentrations ($x = 0.0625$, 0.125, and 0.25) and $Ga_{1-x}TM_xP$ (TM = Cr and Mn) at ($x = 0.0625$ and 0.125) compounds are half-metallic ferromagnets (HMF) with 100 % spin polarization at the Fermi level. The HMF character destroyed for $Ga_{1-x}Cr_xP$ and $Ga_{1-x}Mn_xP$ at higher concentration $x = 0.25$. The HMF behavior is confirmed by the integral Bohr magneton of total magnetic moments of 2, 3, and 4 μ_B respectively for V, Cr, and Mn doping systems, and the HMF materials exhibit high half-metallic gaps at low concentration $x = 0.0625$ of V, Cr, and Mn. Therefore, the $Ga_{1-x}TM_xP$ DMSs at low concentrations (x) of (TM = V, Cr, and Mn) seem to be promising candidates for possible spintronic applications.

References

1. Kılıç, A., Kervan, N., Kervan, S.: J. Supercond. Nov. Magn. **28**, 1767 (2015)
2. Wolf, S.A. et al.: Science **294**, 1488 (2001)
3. Žutić, I., Fabian, J., Das Sarma, S.: Rev. Mod. Phys. **76**, 323 (2004)
4. Doumi, B., Tadjer, A., Dahmane, F., Djedid, A., Yakoubi, A., Barkat, Y., Ould Kada, M., Sayede, A., Hamada, L.: J. Supercond. Nov. Magn. **27**, 293 (2014)
5. de Groot, R.A., Mueller, F.M., van Engen, P.G., Buschow, K.H.J.: Phys. Rev. Lett. **50**, 2024 (1983)
6. Mokaddem, A., Doumi, B., Sayede, A., Bensaid, D., Tadjer, A., Boutaleb, M.: J. Supercond. Nov. Magn. **28**, 157 (2015)
7. Sharma, V., Manchanda, P., Sahota, P.K., Skomski, R., Kashyap, A.: J. Magn. Magn. Mater. **324**, 786 (2012)
8. Huang, H.M., Luo, S.J., Yao, K.L.: Phys. Status Solidi B **248**, 1258 (2011)
9. Saini, H.S., Singh, M., Reshak, A.H., Kashyap, M.K.: J. Alloy. Compd. **536**, 214 (2012)
10. Ahmad, I., Amin, B.: Comput. Mater. Sci. **68**, 55 (2013)
11. Haneef, M., Arif, S., Akbar, J., Abdul-Malik, A.: J. Electron. Mater. **43**, 3169 (2014)
12. Yao, G., Fan, G., Zheng, S., Ma, J., Chen, J., Zhou, D., Li, S., Zhang, Y., Su, S.: Opt. Mater. **34**, 1593 (2012)
13. Yao, G., Fan, G., Xing, H., Zheng, S., Ma, J., Zhang, Y., He, L.: J. Magn. Magn. Mater. **331**, 117 (2013)
14. Zaari, H., Boujnah, M., Labrim, H., Khalil, B., Benyoussef, A., El Kenz, A.: J. Supercond. Nov. Magn. **26**, 2961 (2013)
15. Doumi, B., Tadjer, A., Dahmane, F., Mesri, D., Aourag, H.: J. Supercond. Nov. Magn. **26**, 515 (2013)
16. Sajjad, M., Zhang, H.X., Noor, N.A., Alay-e-Abbas, S.M., Shaukat, A., Mahmood, Q.: J. Magn. Magn. Mater. **343**, 177 (2013)
17. Dahmane, F., Tadjer, A., Doumi, B., Mesri, D., Aourag, H.: J. Supercond. Nov. Magn. **26**, 3339 (2013)

18. Boutaleb, M., Tadjer, A., Doumi, B., Djedid, A., Yakoubi, A., Dahmane, F., Abbar, B.: J. Supercond. Nov. Magn. **27**, 1603 (2014)
19. Liang, P., Liu, Y., Hu, X.H., Wang, L., Dong, Q., Jing, X.: J. Magn. Magn. Mater. **355**, 295 (2014)
20. Dahmane, F., Tadjer, A., Doumi, B., Mesri, D., Aourag, H., Sayede, A.: Mater. Sci. Semicond. Process. **21**, 66 (2014)
21. Sajjad, M., Zhang, H.X., Noor, N.A., Alay-e-Abbas, S.M., Younas, M., Abid, M., Shaukat, A.: J. Supercond. Nov. Magn. **27**, 2327 (2014)
22. Doumi, B., Mokaddem, A., Ishak-Boushaki, M., Bensaid, D.: Sci. Semicond. Process. **32**, 166 (2015)
23. Boutaleb, M., Doumi, B., Sayede, A., Tadjer, A., Mokaddem, A.: J. Supercond. Nov. Magn. **28**, 143 (2015)
24. Sajjad, M., Manzoor, S., Zhang, H.X., Noor, N.A., Alay-e-Abbas, S.M., Shaukat, A., Khenata, R.: J. Magn. Magn. Mater. **379**, 63 (2015)
25. Arda, L., Açıkgöz, M., Güngör, A.: J. Supercond. Nov. Magn. **25**, 2701 (2012)
26. Singh, J., Verma, N.K.: J. Supercond. Nov. Magn. **25**, 2425 (2012)
27. Borges, R.P., Ribeiro, B., Cruz, M.M., Godinho, M., Wahl, U., da Silva, R.C., Gonçalves, A.P., Magén, C.: Eur. Phys. J. B **86**, 254 (2013)
28. Wang, F., Huang, W.W., Li, S.Y., Lian, A., Zhang, X.T., Cao, W.: J. Magn. Magn. Mater. **340**, 5 (2013)
29. Singh, J., Kumar, S., Verma, N.K.: Mater. Sci. Semicond. Process. **26**, 1 (2014)
30. Babu, B., Aswani, T., Rao, G.T., Stella, R.J., Jayaraja, B., Ravikumar, R.V.S.S.N.: J. Magn. Magn. Mater. **355**, 76 (2014)
31. Al-Douri, Y., Reshak, A.H.: Appl. Phys. A **104**, 1159 (2011)
32. Pyshkin, S.L., Ballato, J., Chumanov, G.: J. Opt. A: Pure Appl. Opt. **9**, 33 (2007)
33. Dietl, T., Ohno, H., Matsukara, F., Cibert, J., Ferrand, D.: Science **287**, 1019 (2000)
34. Tarhan, E., Miotkowski, I., Rodriguez, S., Ramdas, A.K.: Phys. Rev. B **67**, 195202 (2003)
35. Scarpulla, M.A., Cardozo, B.L., Farshchi, R., Hlaing Oo, W.M., McCluskey, M.D., Yu, K.M., Dubon, O.D.: Phys. Rev. Lett. **95**, 207204 (2005)
36. Owens, F.J.: J. Phys. Chem. Solids **66**, 793 (2005)
37. Hohenberg, P., Kohn, W.: Phys. Rev. B **136**, 864 (1964)
38. Kohn, W., Sham, L.J.: Phys. Rev. A **140**, 1133 (1965)
39. Wu, Z., Cohen, R.E.: Phys. Rev. B **73**, 235116 (2006)
40. Blaha, P., Schwarz, K., Madsen, G.K.H., Kvasnicka, D., Luitz, J.: WIEN2k, An augmented plane wave plus local orbitals program for calculating crystal properties. Vienna University of Technology, Vienna (2001)
41. Monkhorst, H.J., Pack, J.D.: Phys. Rev. B **13**, 5188 (1976)
42. Pack, J.D., Monkhorst, H.J.: Phys. Rev. B **16**, 1748 (1977)
43. Muranghan, F.D.: Proc. Natl. Acad. Sci. U.S.A. **30**, 244 (1944)
44. Tran, F., Laskowski, R., Blaha, P., Schwarz, K.: Phys. Rev. B **75**, 115131 (2007)
45. Heyd, J., Peralta, J.E., Scuseria, G.E., Martin, R.L.: J. Chem. Phys. **123**, 174101 (2005)
46. Wang, S.Q., Ye, H.Q.: Phys. Rev. B **66**, 235111 (2002)
47. Perdew, J.P., Burke, K., Ernzerhof, M.: Phys. Rev. Lett. **77**, 3865 (1996)
48. Sharma, S., Verma, A.S., Bhandari, R., Kumari, S., Jindal, V.K.: Mater. Sci. Semicond. Process **27**, 79 (2014)
49. Yao, K.L., Gao, G.Y., Liu, Z.L., Zhu, L.: Solid State Commun. **133**, 301 (2005)
50. Gao, G.Y., Yao, K.L., Şaşıoğlu, E., Sandratskii, L.M., Liu, Z.L., Jiang, J.L.: Phys. Rev. B **75**, 174442 (2007)
51. Doumi, B., Mokaddem, A., Temimi, L., Beldjoudi, N., Elkeurti, M., Dahmane, F., Sayede, A., Tadjer, A., Ishak-Boushaki, M.: Eur. Phys. J. B **88**, 93 (2015)
52. Sato, K., Dederichs, P.H., Araki, K., Katayama-Yoshida, H.: Phys. Status Solidi C **7**, 2855 (2003)
53. Sato, K., Katayama-Yoshida, H.: Jpn. J. Appl. Phys. **40**, L485 (2001)
54. Sato, K., Katayama-Yoshida, H., Dederichs, P.H.: J. Supercond. **16**(1), 31 (2003)
55. Akai, H.: Phys. Rev. Lett. **81**, 3002 (1998)